Infrared Reflection–Absorption Spectrometry of Monolayer Films at the Air–Water Interface

Richard Mendelsohn and Carol R. Flach
Rutgers University, Newark, NJ, USA

1 INTRODUCTION

Monolayers at the air–water interface provide an important and convenient model experimental system for investigating both chemical and biological problems. For chemists interested in molecular structure determination, the air–water interface permits effective control of many experimental variables including temperature, film and subphase compositions, phase state of the film-forming molecules, lateral pressure, average distance between molecules, surface viscosity and domain size and shape. For biologists, monolayers at the air–water interface provide an experimentally accessible and reasonably realistic model for a variety of in vivo processes including the function of pulmonary surfactant, the interaction of peptides and extrinsic membrane proteins with biological membranes, and the mechanism of enzyme-mediated interfacial catalysis.

Despite the fact that monolayers have been utilized as a simple and powerful experimental model system for over half a century, the acquisition of structural information from them has proven to be a significant challenge. The reason for this is fairly obvious. Until the early 1980s, techniques with an adequate combination of sensitivity and/or spatial resolution to provide information about domain formation and molecular structure were not available. Prior to development of spectroscopic methods for the characterization of films at a variety of distance scales, structural information was traditionally extracted from the measurement of surface pressure–molecular area (π–A) isotherms.

The molecules used to constitute the films are traditionally amphiphiles ranging from long chain fatty acids through phospholipids, which produce insoluble monolayers. A typical π–A isotherm is shown for a monolayer film of dimyristoylphosphatidic acid (DMPA) in Figure 1. When such a film initially in the gas (G) phase is compressed, a liquid expanded (LE) phase results. Further compression produces the liquid condensed (LC) or tilted condensed phase which is formed via a first-order transition represented by the horizontal line on the isotherm. Within this plateau region, LC and LE phases coexist. At higher pressures, a transition from LC to a solid (S) or untilted condensed phase occurs. Eventually, at the highest pressure, the monolayer breaks down and a collapsed state of heterogeneous structure results.

In the early 1980s epifluorescence microscopy was developed to study surface phases and domain formation in aqueous monolayers. In addition, X-ray diffraction measurements were initiated to provide information about molecular tilt angles and packing. More recently, Brewster angle microscopy has provided a means for imaging domains without the requirements for fluorophore incorporation. Additional methods providing information about transport and molecular properties are less frequently used. The various approaches are summarized in Table 1.

While information about the domains and phases formed by amphiphiles provides an indispensable characterization of these systems, such data do not provide a complete molecular level description of monolayer films. To acquire structural information such as chain conformation, hydrogen bonding and ionic interactions in amphiphiles, and secondary structure and orientation in proteins, vibrational spectroscopic techniques are required (see Table 1), the most powerful of which is a variant of infrared (IR) spectroscopy known as infrared reflection–absorption spectroscopy (IRRAS).

© John Wiley & Sons Ltd, 2002.

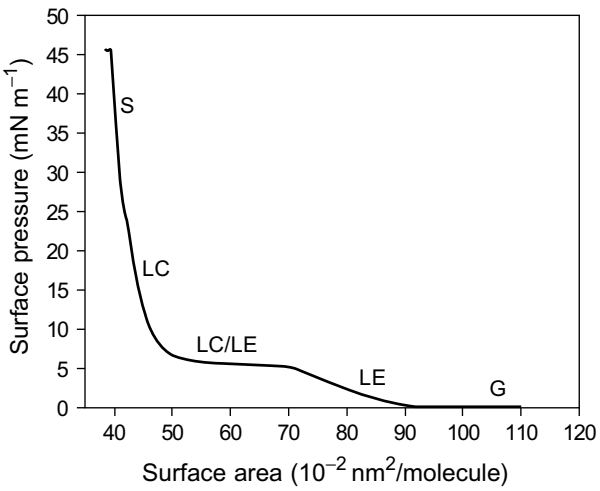

Figure 1. Surface pressure–molecular area (π–A) isotherm for DMPA on 100 mM NaCl, 2 μM EDTA H_2O-based subphase at 21 °C. A compression rate of 2.27×10^{-2} nm^2(molecule min)$^{-1}$ was used.

The inherent advantages of IR spectroscopy for the molecular structure characterization of lipids and proteins are well known. The technique detects molecular vibrations accompanied by changing molecular dipole moments. The vibrational frequencies that are detected are sensitive to molecular conformation. An additional advantage of the approach is that isotopic labeling experiments may be used to obtain structural information from particular molecular functional groups. The structural information currently available from IRRAS studies of chain molecules is summarized in Table 2. The spectra–structure correlations presented, especially those for chain molecules, are to a large extent based on the seminal bulk phase studies of Snyder *et al*. at Berkeley.

Table 1. Techniques for structural investigation of aqueous monolayers.

Physical Method	Structural Information
Pressure–area isotherms	Surface thermodynamics, molecular areas, phase transitions
Surface viscosity	Viscoelasticity
Ellipsometry	Film optical constants, phase transitions
Brewster angle microscopy	Domain structure and size distribution
Fluorescence microscopy	Domain organization of labeled species
X-ray reflectivity	In-plane molecular order, molecular orientation, and subcell structure
Sum frequency generation	Chain conformational order
Second harmonic generation	Chain conformational order
IRRAS	Chain conformation and orientation, protein secondary structure and functional group orientation

Dluhy and Cornell[1,2] were the first to acquire IRRAS spectra from aqueous Langmuir films of fatty acids and phospholipids. These experiments were a technological triumph in which two formidable obstacles were overcome. First, IR absorption bands of biological molecules are relatively weak, extinction coefficients being 0.1 to 5% of their electronic counterparts. Second, the reflection properties of water in the IR are poorly suited to IRRAS experiments. A third difficulty addressed by other laboratories in later studies, arises in IRRAS investigations of proteins. It happens that the intense absorptions of both the liquid and

Table 2. IR modes used for IRRAS analysis of amphiphiles.

Mode	Frequency range (cm^{-1})	Comment
Chain modes		
CH_2 sym. stretch	2849–2854	The frequencies are qualitative markers of conformational disorder
CH_2 asym. stretch	2916–2924	
CD_2 sym.stretch	2090–2100	
CD_2 asym.stretch	2195–2200	
CH_2 scissoring	1462,1474	Orthorhombic phase doublet
	1468	Hexagonal or triclinic phase
CD_2 scissoring	1086,1094	Orthorhombic phase doublet
	1089	Hexagonal or triclinic phase
Polar region vibrations		
PO_2^- asym. stretch	1220–1250	This frequency is sensitive to ion binding and hydration
PO_2^- sym. stretch	1090	
C=O stretch of fatty acids	1690–1740	This frequency is sensitive to protonation state
C=O stretch of esters	1710–1740	This frequency is sensitive to hydration and hydrogen bonding

vapor phases of H_2O mask the vibrations of three important protein vibrational modes, namely the Amide A (peptide bond N–H stretch), Amide I (peptide bond C=O stretch) and Amide II (a mixed normal mode consisting predominantly of peptide bond N–H in-plane bending and C–N stretching internal coordinates). The methods used to overcome this obstacle are of central importance in IRRAS and are discussed below. In the past decade, IRRAS techniques have steadily improved. Alternatives to the initial instrumentation have been implemented and while the experiment cannot yet be termed routine, the technological difficulties can be surmounted. A variety of applications addressing the structure and orientation of peptides and proteins have appeared. Sufficient sensitivity is available to permit the use of isotopic labels providing information about particular molecular regions in one component or mixed monolayers. Theoretical models for determination of molecular orientation have been refined and tested. IRRAS thus appears poised to take its place as a unique method for the determination of molecular structure at aqueous interfaces. The current article will summarize some of the experimental procedures used to acquire IRRAS data, outline and provide examples of the theoretical methods used for evaluation of intensities which yield orientation information, and summarize the applications to date (as of February 2000). We have attempted to represent the contributions of the various groups around the world involved in this research area. Three review articles have recently appeared, and readers are encouraged to examine these.[3–5]

2 EXPERIMENTAL

2.1 Instrument design

A schematic of the IRRAS system at Rutgers University is shown in Figure 2. While the instrumental components are sufficiently versatile so that details may vary between systems, it is incumbent on the experimenter to incorporate several design features, as follows:

- For the most accurate determination of tilt angles, optics (reflective) for handling the incident IR radiation must be adjustable so that the aqueous surface may be illuminated at a variety of incident angles.
- The Langmuir trough containing the monolayer films must be of sufficient size ($\geq$6 cm for Teflon®) to minimize the effects of meniscus formation. In addition, troughs ought to incorporate an adjustable barrier, a port for injection into the subphase, and a Wilhelmy plate or equivalent for surface pressure determination. The subphase temperature should be controlled to better than $\pm 0.5\,^{\circ}$C, to keep the vapor pressure of water as constant as possible and to minimize the influence of varying temperature on the monolayer constituents.
- The optical path should have a position for a polarizer. The polarizer should be of the highest quality available. This issue is more critical than for polarized transmission or attenuated total reflection (ATR) experiments, for the following reason. Unlike conventional experiments where the p- (parallel) and s- (perpendicular) components of the transmitted intensity are approximately equal, the IRRAS intensities of the two reflected components are dramatically different. Close to the Brewster angle, the intensity of the reflected p-polarized light is minimized so that the reflected intensity of the s-polarized component may become 100-fold greater than that of the p-polarized. Under such conditions, in a polarization experiment, if the polarizer is 99% efficient, and if the experiment is arranged to detect p-polarized light, 1% of s-polarized light will leak into the p-channel. Ostensibly "p-polarized" light will then in fact contain an s-polarized component of equal intensity. The situation worsens for poorer quality polarizers. The efficiency of the polarizer must therefore be determined across the mid-IR range.
- For polarization measurements, the angular divergence of the incident light ought to be controlled to $<1^{\circ}$. Iris diaphragms are useful for this purpose. This is especially important for incident angles close to the Brewster angle (about 53° for water).

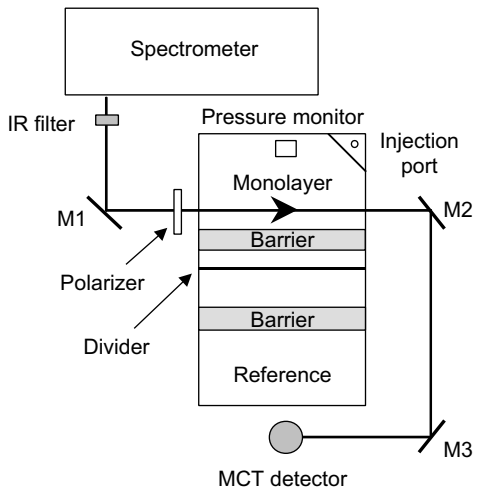

Figure 2. Schematic of an IRRAS instrument. The bold line marks the IR beam path. M1, M2, and M3 are off-axis parabolic mirrors. The distance between M1 and the water surface is set at the focal length of the mirror (120 mm), as is the distance between the water surface and M2. The injection port allows for injection of soluble proteins or ions into the subphase without disturbing a pre-existing monolayer. The divider and dual barriers minimize diffusion between the reference and film side of the trough while allowing for further film compression.

- The entire setup must be enclosed and purged to keep the relative humidity levels as low and as constant as is feasible. As noted above, interference from the water vapor signal is the main experimental obstacle to acquisition of good IRRAS spectra from protein monolayers. Substitution of D_2O for H_2O in the subphase does not eliminate the problem, as atmospheric water vapor must be purged from the system and HDO (produced by D → H exchange) possesses rotation–vibration bands that severely overlap protein Amide I and II regions.
- Sakai and Umemura[6] have demonstrated that the incident IR radiation heats the aqueous surface to the point where molecules in expanded phases may be driven from areas of the monolayer being illuminated, thus resulting in lower IRRAS intensities than anticipated. Optical filters absorbing most of the IR radiation in regions not of interest are available. Their insertion into the beam path helps alleviate the heating problem.

2.2 Water vapor compensation

A water subphase ensures the presence of substantial levels of intense water vapor rotation–vibration bands. Substitution with a D_2O subphase lessens, but does not eliminate the interference. The occurrence of water vapor bands is particularly troublesome in the 1400–1800 cm^{-1} region, since that frequency range contains a variety of spectral features of interest in long chain amphiphiles and proteins (see Table 2). Consequently, a great deal of attention has been given to elimination of the water vapor signal. Two approaches have evolved.

Flach *et al.*[7] developed a straightforward sample shuttle approach in which two Langmuir troughs are used in tandem. The first contains the film-covered surface (sample channel); the second contains only the subphase (reference channel). A computer controlled direct drive (servo) motor is used to shuttle the samples in alternating fashion in and out of the IR beam. Signals from the light reflected from each trough are co-added into separate channels. The approach minimizes the effect of humidity variations during the course of the experiment. The advantage of this device is shown in Figure 3. In the Figure, the IRRAS spectrum of the lung surfactant protein, SP-B, is shown without (Figure 3A, 2048 scans) and with (Figure 3B, 1024 scans) water vapor compensation. Although an attempt was made to improve the signal-to-noise ratio in the former case by increasing the number of scans acquired, the Amide I mode remains overlapped by many sharp features arising from the rotation–vibration spectrum of water. These features are reduced by an order of magnitude as a result of the dual channel shuttle operation. With the use of the shuttle system, protein Amide I features as weak as 0.0003 reflectance–absorbance (RA) units may be consistently detected.

Figure 3. IRRAS spectra of lung surfactant protein, SP-B, monolayer at surface pressure of 12 mN m^{-1} on a D_2O buffer (pD 7). The bottom spectrum was acquired by co-adding 8 blocks of 128 scans. The spectra are shown without water vapor subtraction and without smoothing. Shuttling allows the frequency of the Amide I mode to be determined more accurately due to better water vapor compensation. The Amide I band in the bottom spectrum was found at 1645 cm^{-1} using a center of gravity algorithm.

The second approach, developed by Blaudez *et al.*[8] uses a polarization modulation technique and is termed polarization modulation infrared reflection–absorption spectroscopy (PM-IRRAS). The polarization of the incident electric field is rapidly modulated between the s and p channels, and reflected from the water surface. The reflected beam signal is electronically filtered and demodulated with a lock-in amplifier. Following Fourier transformation, a differential reflectivity spectrum is computed as $(\Delta R/R) = (R_p - R_s)/(R_p + R_s)$. A detailed discussion has been presented by Buffeteau *et al.*[9]

Each method of water vapor suppression has its advantages and disadvantages. The incorporation of a shuttle system is technically straightforward, easily automated, and requires minimal modifications of the optical path of the spectrometer. The presence of a dual trough system tends to enlarge the volume that has to be purged, and to increase equilibration times. In addition, the shuttle should be operated with a direct drive motor at sufficiently slow speeds to preclude disturbance of the film. PM-IRRAS requires the incorporation of additional elements in the optical system which tend to diminish the throughput. In addition, the polarization modulation efficiency is perfect only at a single frequency, so that complete compensation of water vapor

cannot be achieved in practice. Also, since PM-IRRAS suppresses signals from randomly oriented film constituents, vibrations from randomly oriented species will be detected with reduced efficiency or not at all. Lastly, use of the method for quantitative determination of molecular orientation is limited. This application requires measurement at a variety of tilt angles. Realignment of the PM-IRRAS optics to routinely change the angle of incidence is evidently nontrivial since it has not yet been reported.

2.3 Experimental caveats

It has been known for many years that the physical state of the monolayer may be drastically affected by the means by which the monolayer is formed and compressed. Ideally, when acquiring isotherms for insoluble monolayers, the molecules are spread over a large enough surface area so that the surface pressure is less than the equilibrium spreading pressure. In reality, this is not always possible due to the nature of the film constituents and experimental constraints such as trough design and aspect ratio (maximum/minimum surface area). Pallas and Pethica[10] reported on the variations in π–A isotherms that result from different film spreading and compression methods, in an effort to resolve the controversy concerning the order of the LE/LC phase transition for long chain carboxylic acids. Subsequently, Gericke *et al.*[11,12] used IRRAS to investigate differences in molecular structure resulting from the application of two particular spreading and compression techniques. In the first technique, referred to as the single shot method, the monolayer is sampled at a single molecular area after spreading a known amount to a fixed surface area. This process is repeated, i.e. a new monolayer is spread, to cover a range of molecular areas and corresponding surface pressure values. In the second technique, the discontinuous compression method, a monolayer is spread at a large molecular area and the barrier is moved to a particular location where measurements are begun only after the pressure has become constant. This process is repeated as positions along a π–A isotherm are sampled. Gericke *et al.*[11,12] observed smaller acyl chain tilt angles for monolayers of 1-hexadecanol prepared by the single shot method compared to discontinuous compression even after allowing 80 min for film relaxation. In both cases, the methylene stretching frequencies indicated substantial acyl chain conformational order. Similar experiments with the phospholipid 1,2-dipalmitoylphosphatidylcholine (DPPC) show different behavior than the alcohol. DPPC monolayers spread in the LC/LE coexistence region using the single shot method relax to an ordered state in terms of tilt angle and acyl chain conformation without, however, ever reaching the same degree of conformational order as when discontinuous compression is applied. These experiments demonstrate the strong dependence of physical state on monolayer spreading and compression techniques.

2.4 Interpretation of experimental data

2.4.1 Frequencies

The traditional approaches for interpretation of IR spectra of large molecules may in large part be utilized for interpretation of IRRAS data. These methods utilize the long history of spectra–structure correlations established for small molecules, bolstered by normal coordinate calculations. The assumption is routinely made that the spectra–structure correlations persist in going from the small molecules to the biopolymer. However, allowance must be made for the occurrence of coupling between identical (or at least very similar) oscillators which produces characteristic splittings of spectral features or broadening of spectral lines. This effect is not an esoteric theoretical oddity, but in fact provides direct structural information from monolayer films. Two examples, one each from lipid[13] and protein spectroscopy[7] are cited here.

Lipids are amphipathic molecules possessing long chain hydrocarbon segments. The CH_2 scissoring vibrations near 1465 cm^{-1} from such species have been observed to couple and split in characteristic fashion if and only if the chains are conformationally ordered and packed in an orthorhombic perpendicular geometry. A spectral doublet appears (1462, 1474 cm^{-1}) under these conditions. The observation of the doublet for behenic acid methyl ester monolayer films (Figure 4) immediately and unambiguously defines the structure of the phase.

In a similar vein, when peptides or proteins adopt regular secondary structures, the Amide I (peptide bond C=O stretch) mode splits in a characteristic fashion. The most dramatic splitting occurs for the antiparallel β-sheet conformation. The Amide I vibration (near 1650 cm^{-1} for *N*-methylacetamide) is highly perturbed due to inter- and intrachain interactions, and transition dipole (through space) coupling. The IR active modes resulting from these interactions produce a strong band at 1630 cm^{-1} and a 5 to 10-fold weaker feature near 1680 cm^{-1}, which are immediately diagnostic for this secondary structure. An example is the IRRAS spectrum of a synthetic antiparallel β-sheet sheet peptide shown in Figure 5.

In most instances, the nature of the structural information from IR frequencies of large molecules is much more qualitative and empirical. For example, the frequencies (both symmetric and asymmetric) of the methylene stretching vibrations are routinely used to characterize the state of conformational order in chain amphiphiles. It has been

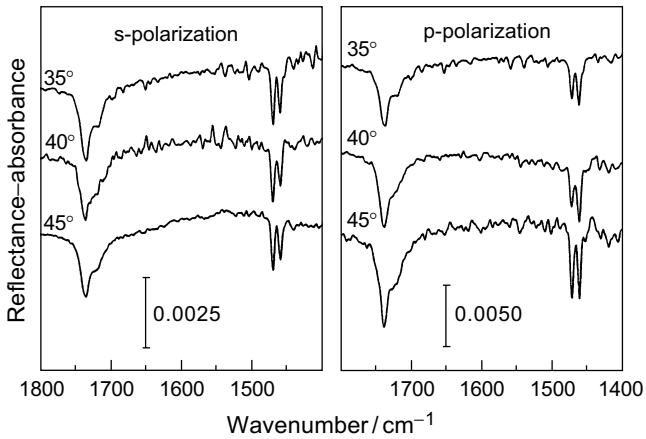

Figure 4. IRRAS spectra of behenic acid methyl ester monolayers at surface pressure of 14 mN m^{-1} on D_2O subphase for different angles of incidence as noted. A shuttle system and polarized radiation was used. The ester carbonyl band is observed at ~1737 cm^{-1} with a smaller shoulder at ~1720 cm^{-1} indicating that the majority of the carbonyl groups are unprotonated (band at 1737 cm^{-1}). Splitting in the methylene scissoring mode produces the two components near 1472 and 1463 cm^{-1}. This observation identifies an orthorhombic phase with an acyl chain tilt angle of 0°.

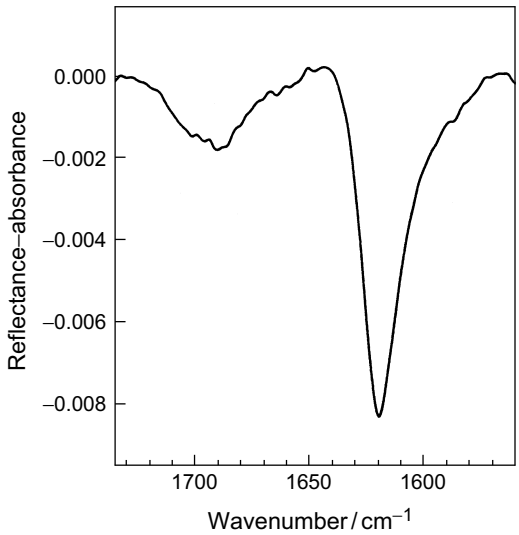

Figure 5. The IRRAS spectrum of a surface active peptide designed to adopt an antiparallel β-sheet structure at the air–water interface. The spectrum was acquired at surface pressure of 18 mN m^{-1} on D_2O subphase using a shuttle system. The Amide I band is split into two components, at ~1620 and 1689 cm^{-1}, which indicate that the secondary structure of this peptide in situ is antiparallel β-sheet.

observed during the gel → liquid crystal transition in (bulk phase) lipid vesicle dispersions that the symmetric CH_2 stretching frequency increases from ~2848 to 2853 cm^{-1}. Thus, a lipid in a conformationally ordered state is characterized by a CH_2 stretching mode below ~2850 cm^{-1}, with conformational disorder leading to a frequency several cm^{-1} higher. This qualitative result is straightforward; it

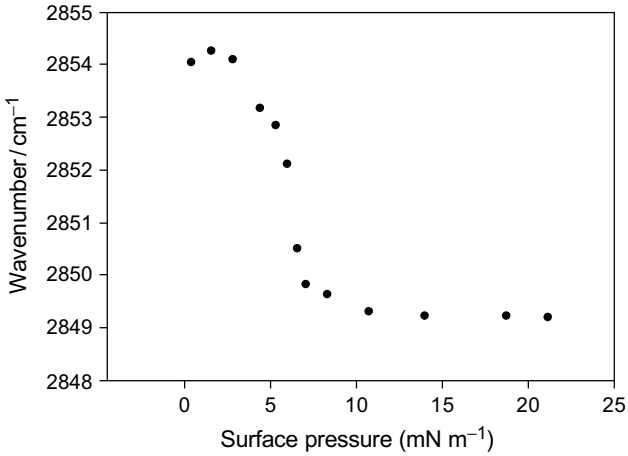

Figure 6. Surface pressure versus frequency of the methylene symmetric stretching vibration for a DMPA monolayer on H_2O subphase during intermittent compression.

has proven difficult, however, to quantitatively correlate the exact wavenumber position with the extent of disorder. In general, the increase in this frequency arises from an increase in the C–H stretching force constant for a C–H bond trans to a C–C bond (therefore in a gauche conformational state with respect to the carbon skeleton chain). The variation of ν_{sym} CH_2 along the π–A isotherm for DMPA is shown in Figure 6. The LE and G phases are characterized by high levels of chain conformational disorder ($\pi <$ 5 mN m^{-1}). Conformational ordering is manifest during the LE–LC transition during which a 3–4 cm^{-1} reduction in ν_{sym} CH_2 is observed over a small range of pressures. The lipid acyl chains in the LC phase ($\pi >$ 6 mN m^{-1}) appear to be nearly all-trans. Little further change is noted upon continuing compression.

A cautionary note is in order at this point. Band positions measured in IRRAS may differ from those observed in transmission.[3] In general, the effects arise from the optical properties of the substrate and are small especially when using unpolarized radiation. These shifts should be simulated when using polarized radiation by applying standard theoretical approaches.

2.4.2 *Intensities*

In general, band intensities are harder to measure accurately in vibrational spectroscopy than frequencies; in addition, their interpretations are more difficult. Nevertheless, a main advantage of IRRAS is that molecular and functional group orientation may be determined from comparisons of experimentally measured intensities with any one of several essentially equivalent theoretical models. The problem may be stated succinctly. We are attempting to measure the tilt of ordered regions within molecules (with respect to the surface normal) that are tens of angstroms long, using a measuring device (IR radiation) that is micrometers long.

A brief description of how this task is accomplished using a particular theoretical model follows.

2.5 Determination of tilt angles by IRRAS

IRRAS data are reported as plots of RA versus wavenumber. RA is the $-\log_{10}(R/R_o)$ where R is the reflectivity of the film-covered surface and R_o is the reflectivity of the water. RAs may be positive or negative depending on the state of polarization of the incident light, the proximity of the angle of incidence to the Brewster angle, and the direction of the change in the dipole moment during the normal mode. By consideration of the reflection properties of light from a three layer (air–film–water) interface, it is feasible to determine the angle of orientation of transition moments with respect to the surface. The various theoretical approaches have been reviewed adequately elsewhere.[3] We have selected the equations of Kuzmin *et al.*[14,15] However, computer analysis of various descriptions based on Schopper's equations[16] and more recently due to Yamamoto and Ishida[17,18] have produced the same results to 0.25%, which is better than the available experimental precision.

2.5.1 *Definitions of optical parameters*

The fraction of light reflected at an interface depends on the mismatch between the optical constants of the two phases. For an absorbing, isotropic medium, two parameters describe its optical properties at each point. The real refractive index, n, and the extinction coefficient, k. These are taken together as a complex refractive index $\underline{\underline{n}} = n + \mathrm{i}k$ (the double underlining indicates a complex quantity).

The theory uses the conventional definitions of plane polarized radiation. Parallel (p) polarized radiation has the electric vector oscillating in the plane of incidence while perpendicular (s) polarized radiation has the electric vector perpendicular to the plane of incidence. The z axis is chosen normal to the interface, and the x axis is located so that the plane of incidence is the x,z plane. p-Polarized radiation thus has x and z components. s-Polarized radiation only has a y Cartesian component.

2.5.2 *The Fresnel equations for reflection*

The Fresnel equations for a two-phase system, i.e. an air–water interface, can be derived from electric field amplitude ratios for s- and p-polarization and Snell's law. The reflection coefficients, $\underline{\underline{r}}_s$ and $\underline{\underline{r}}_p$, can then be calculated from the Fresnel equations:
for s-polarization:

$$\underline{\underline{r}}_s = \frac{\sin\left(\phi_1 - \underline{\underline{\phi}}_2\right)}{\sin\left(\phi_1 + \underline{\underline{\phi}}_2\right)} \tag{1}$$

and for p-polarization:

$$\underline{\underline{r}}_p = \frac{\tan\left(\phi_1 - \underline{\underline{\phi}}_2\right)}{\tan\left(\phi_1 + \underline{\underline{\phi}}_2\right)} \tag{2}$$

where ϕ_1 is the angle of incidence between the incoming ray and the direction of the surface normal and $\underline{\underline{\phi}}_2$ is the complex angle of the refracted ray.

2.5.3 *Modifications for anisotropic molecular orientation*

The addition of an absorbing, anisotropic film must be incorporated into the theoretical models. Phospholipid acyl chains provide an example of the anisotropy present in the films. The long axes of the acyl chains, nearly normal to the water substrate, have transition dipoles for the CH_2 stretching modes that are almost parallel to the interface. Thus, for these vibrations the extinction coefficient of the film has strong x and y components and a weak z component. The film is also assumed to be uniaxial, achieved by free rotation of the molecular axis about the surface normal and free rotation of the molecules about their own axes. To account for both considerations, the equations must explicitly include $\underline{\underline{n}}_x = \underline{\underline{n}}_y$ and $\underline{\underline{n}}_z$ for the film phase. The reflection coefficients of a thin anisotropic film have been given by Kuzmin *et al.*,[14,15] as follows:
for s-polarization:

$$\underline{\underline{r}}_s = -\frac{\sin\left(\phi_1 - \underline{\underline{\phi}}_2\right) - ik_0\underline{\underline{n}}_2^{-1}\sin\phi_1\underline{\underline{I}}_1}{\sin(\phi_1 + \phi_2) - ik_0\underline{\underline{n}}_2^{-1}\sin\phi_1\underline{\underline{I}}_1} \tag{3}$$

for p-polarization:

$$\underline{\underline{r}}_p = \frac{\sin\left(\phi_1 - \underline{\underline{\phi}}_2\right)\cos\left(\phi_1 + \underline{\underline{\phi}}_2\right) - ik_0\underline{\underline{n}}_2^{-1}\sin\phi_1\left(\underline{\underline{I}}_1\cos\phi_1\cos\underline{\underline{\phi}}_2 - \underline{\underline{I}}_2\sin\phi_1\sin\underline{\underline{\phi}}_2\right)}{\sin\left(\phi_1 + \underline{\underline{\phi}}_2\right)\cos\left(\phi_1 - \underline{\underline{\phi}}_2\right) - ik_0\underline{\underline{n}}_2^{-1}\sin\phi_1\left(\underline{\underline{I}}_1\cos\phi_1\cos\underline{\underline{\phi}}_2 + \underline{\underline{I}}_2\sin\phi_1\sin\underline{\underline{\phi}}_2\right)} \tag{4}$$

In which

$$\underline{\underline{I}}_1 = \int\left(\underline{\underline{n}}_x^2(z) - \underline{\underline{n}}_2^2\right)\mathrm{d}z \tag{5}$$

$$\underline{\underline{I}}_2 = \int\frac{\underline{\underline{n}}_z^2(z) - \underline{\underline{n}}_2^2}{\underline{\underline{n}}_z^2(z)}\mathrm{d}z \tag{6}$$

and

$$k_o = \frac{2\pi}{\lambda} \tag{7}$$

In addition, this treatment allows for variation in the optical properties of the film in the z direction and thus permits, in principle, the inclusion of film inhomogeneity. However, to date no information concerning the profile of the refractive indices is available and constant values for $\underline{\underline{n}}_x$ and $\underline{\underline{n}}_z$ have to be used. Accordingly, the integrals transform to:

$$\underline{\underline{I}}_1 = \left(\underline{\underline{n}}_x^2 - \underline{\underline{n}}_2^2\right) h \tag{8}$$

and

$$\underline{\underline{I}}_2 = \frac{\left(\underline{\underline{n}}_z^2 - \underline{\underline{n}}_2^2\right)}{\underline{\underline{n}}_z^2} h \tag{9}$$

where h is the film thickness.

Finally, the reflectivity values, R and R_o, can be calculated by multiplying the respective reflection coefficient with its complex conjugate so that RA values can be obtained.

2.5.4 *Computer simulations*

Computer simulation consists of substituting the appropriate optical constants into the equations that incorporate molecular anisotropy and comparing the calculated IRRAS bands with those observed experimentally. The following parameters are required to calculate a single RA value: angle of incidence, ϕ_1; mean tilt angle of the molecular axis relative to the surface normal, θ; angle that the transition dipole makes with the molecular axis, α; vacuum wavelength of the light, λ; film thickness, h; indices of refraction and extinction coefficients of the incident and final phases, n_0, n_2, k_0, k_2; and the directional refractive indices and extinction coefficients of the film, n_x, n_z, k_x, and k_z. The optical constants for the film are obtained from the following.

When the mean tilt angle of a molecular axis relative to the surface normal is θ, then

$$n_x = n_y = n_{\text{ext}} \sin^2\theta + n_{\text{ord}} \cos^2\theta \tag{10}$$

$$n_z = n_{\text{ext}} \cos^2\theta + n_{\text{ord}} \sin^2\theta \tag{11}$$

where n_{ext} and n_{ord} are refractive indices corresponding to directions parallel and perpendicular to the direction of the molecular axis. Optical constants for H_2O and D_2O subphases are obtained by interpolation of the values given by Bertie *et al.*[19]

To obtain k_x and k_z, Fraser's equations for uniaxial films[20] are used:

$$k_{x\,\max} = \left[\frac{f(\sin^2\alpha)}{2} + \frac{(1-f)}{3}\right] k_{\max} \tag{12}$$

$$k_{z\,\max} = \left[f\cos^2\alpha + \frac{(1-f)}{3}\right] k_{\max} \tag{13}$$

$$f = \frac{(3\cos^2\theta - 1)}{2} \tag{14}$$

where $k_{\max}$ is the transition dipole strength. To simulate an entire band, a lineshape such as a Lorentzian or Gaussian distribution is assumed for the wavenumber dependence of the film extinction coefficients and refractive indices.

Theoretically, measurements for each polarization at a single angle of incidence should be adequate to determine the unknowns, θ and k. In practice, the uncertainties in intensity measurements of these weak bands render it essential to make measurements at a variety of angles of incidence. The measured intensities are then compared to those predicted from computer simulations for various values of θ and k, to thereby arrive at the value of tilt angle for the particular transition moment under consideration. In addition, the polarization efficiency must be determined.

2.5.5 *Determination of helix orientation*[21]

The determination of transition dipole orientation is illustrated for the pulmonary surfactant protein SP-C. Pulmonary surfactant is a mixture of lipids and proteins that forms a monolayer film at the air–alveolar interface. Its putative function in vivo is to lower surface tension at this interface to reduce the work required to expand lung volume. The pathological consequences of a deficiency in surfactant are severe. Respiratory distress syndrome (RDS) in premature infants is one common condition.

There are four surfactant specific proteins which have been identified. Two of these, SP-B and SP-C, are small hydrophobic species. SP-C has a molecular weight of ~3500 and possesses a predominantly α-helical secondary structure. The in vivo function of this molecule is unknown. In vitro, SP-C is known to facilitate the spreading of surfactant lipids across the air–water interface. The mechanism by which it accomplishes this is unknown. Our approach was to determine the orientation of the helix in both monolayer and bilayer preparations of this species, to delineate a possible mechanism by which SP-C enhanced phospholipid spreading rates.

The primary data are shown in Figures 7 and 8 for the DPPC and SP-C. s-Polarized and p-polarized spectra of the methylene stretching region at three angles of incidence for a condensed DPPC monolayer are shown in

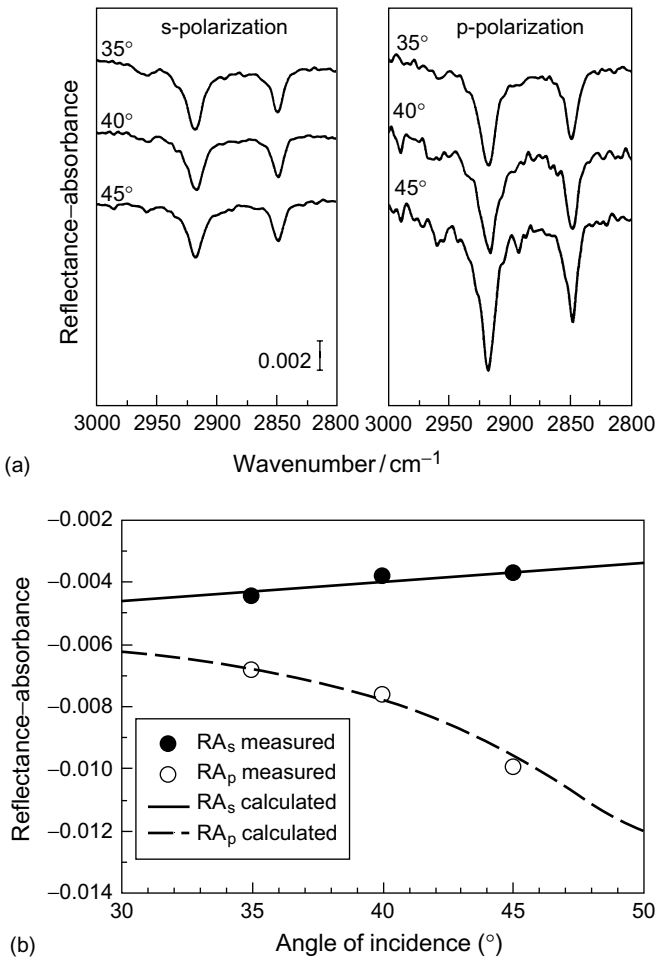

Figure 7. (a) IRRAS spectra of the methylene stretching band region for pure DPPC monolayers on H_2O subphase at 19.0 °C. Spectra were acquired at surface pressure of 28 mN m^{-1} using polarized radiation for the three angles of incidence noted. (b) The simulated and measured RA values for the ν_a CH_2 band minima versus angle of incidence are shown for the pure DPPC monolayer. To calculate the RA values, the real part of the center of the band's refractive index was taken as 1.41, the length of the DPPC molecule as 2.66 nm, and the degree of polarization as 98.7%. The best fit to the experimental data was found using an acyl chain tilt angle of 26°.

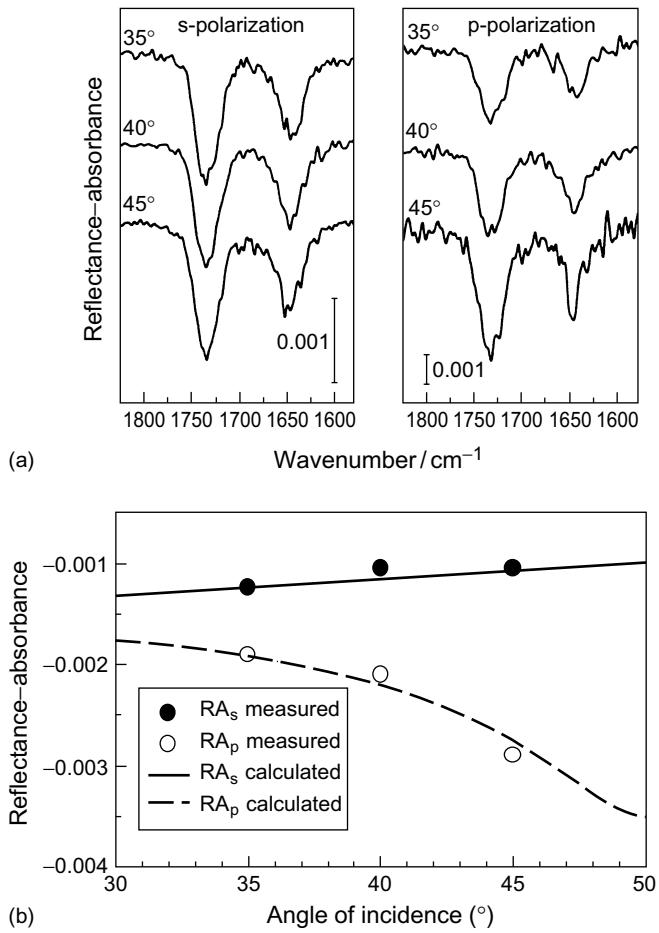

Figure 8. (a) IRRAS spectra of the 1800–1400 cm^{-1} region for DPPC/SP-C (20/1, mol ratio) monolayers on D_2O subphase (19.0 °C) at a surface pressure of 28 mN m^{-1}. Spectra were acquired using polarized radiation at the three angles of incidence noted. The lipid carbonyl band is observed at ~1735 cm^{-1} and the protein Amide I band is at ~1650 cm^{-1}. A shuttle system was used and the spectra shown are not smoothed. (b) The calculated and measured RA values for the Amide I band versus angle of incidence are shown for the DPPC/SP-C monolayer. The real part of the refractive index at the center of the band is 1.41, the length of the protein is 3.41 nm, the degree of polarization is 99.0%, and the angle the transition dipole moment makes with the helix axis is taken as 28°.[22] The best fit was found using a helix tilt angle of 70°.

Figure 7(a). The frequencies of the methylene stretching modes, ($\nu_a(CH_2)$ and $\nu_s(CH_2)$) 2917.9 and 2849.5 cm^{-1}, respectively, are indicative of essentially all-trans conformation in the acyl chains. Similar frequencies were observed for DPPC in the condensed, mixed monolayers with SP-C. An all-trans conformation is a prerequisite for determining the chain orientation. As expected, the variation in intensity of the s-polarized light is small as the Brewster angle is approached. In contrast, the p-polarized component is enhanced by about 50% as the angle of incidence increases from 35 to 45°. These data are sufficient to determine the average tilt angle of the acyl chains as shown in Figure 7(b). The best fit to the data for pure DPPC was obtained for a chain tilt angle of 26° and $k_{max} = 0.54$. In the mixed film with SP-C, the tilt angle for the lipid acyl chains decreased to 10°. Similar data for the lipid carbonyl (~1735 cm^{-1}) and protein Amide I (~1650 cm^{-1}) vibrations of mixed DPPC/SP-C monolayers are shown in Figure 8. The best fit to the data was obtained for a helix tilt angle of 70° and $k_{max} = 0.48$.

Although the signal-to-noise ratio for the SP-C Amide I band is reduced from that for the lipid methylene bands, a detailed examination of the Amide I bandshapes for an α-helical peptide at different tilt angles increases our level

Table 3. Summary of IRRAS applications.

Molecular class	Specific molecule(s)	Structural information	References
Alcohols	$H(CH_2)_{18}$ OH,$F(CF_2)_{10}(CH_2)_2(OH)$	Chain orientation (tilt angle), surface concentration	26, 27
	Dodecanol, tridecanol, tetradecanol	Chain conformation	28
	Stearyl alcohol, heneicoanol (n-$C_{21}H_{43}OH$)	Phase transitions	29, 30
	Hexadecanol	Quantitative chain orientation	81
Fatty acids (and derivatives)	Stearic acid, cadmium stearate and hydroxystearic acid	Chain orientation, effects of heating and airflow	31–33
	Oleic acid	The first observation of IRRAS spectrum	1
	Behenic acid methyl ester	Quantitative chain orientation	13
	Pentadecanoic, hexadecanoic, octadecanoic and octadecenoic acids	Effects of pH on protonation states, COO^-, chain conformation	34–40
	Cadmium arachidate	COO^- and chain orientation	8, 41, 72
	Deuterated palmitic acid/ceramide/cholesterol	Stratum corneum model	51
	Partially deuterated palmitic acids	Differential conformational order in different regions of the molecule	42, 37
	10,12-Pentacosadiyonic acid	Photopolymerization effects on COO^-	43
	2-OH-hexadecanoic acid	Enantiomers vs racemic mixtures, effects of metal ions	37, 42, 79
Phospholipids	DSPC, DMPC and DPPC	Chain conformations (the first report in this area), effects of ions	44–46
	Partially deuterated DPPC, POPC and OPPC	Differential conformational order in different regions of the molecule	47
	DPPC-d_{62} with other phospholipids	Exclusion of species from high pressure monolayers ("squeeze-out" hypothesis), effects of Ca^{2+}, and acyl chain orientation	48–50
	Ceramide/fatty acid/cholesterol	Stratum corneum model	51
Lipid/peptide and lipid/protein	DPPC with pulmonary surfactant proteins (SP-B and SP-C)	Protein secondary structure, "squeeze-out" hypothesis, quantitative helix and lipid acyl chain orientation, effects of SP-C deacylation	21, 52, 63
	DPPC-d_{62}/phosphatidylglycerols/SP-B/SP-C	Effects of proteins on acyl chain conformation	55
	DPPC with phospholipases A_2 and C	Effects of hydrolysis	53, 54
	DPPC and DPPS with melittin	Chain conformation, peptide secondary structure	59
	DPPC and $K_2(LA)_x$ ($x = 6, 8, 10, 12$)	Chain length dependence of secondary structure in monolayers and bulk phases, dependence of secondary structure on spreading conditions	78
	DMPC with melittin or amphipathic synthetic peptide	Structure and orientation of lipid and peptides	24, 25
	DMPC and Gramicidin A	Pressure dependence of helix orientation	23
	DPPC and DPPG with Gramicidin S	Dependence of peptide insertion on lipid phase	80
	1,2-DMPA and Annexin V	Effects of Ca^{2+} on lipid/protein interaction	60, 61
	DPPC or phosphatidylethanolamines and bacterial surface-layer protein	Protein penetration into lipid monolayer	83
Proteins/peptides and synthetic polypeptides	Photosystem II core complex, bacteriorhodopsin, rhodopsin	Dependence of secondary structure on spreading conditions, helix orientation	62, 84, 85
	Amyloid peptide	Secondary structure	82
	Poly(β-benzyl L-aspartate)	Handedness of helices	75, 76
	Poly(ala-gly)$_3$-glu-gly	pH-induced random coil to β-sheet transition	77
	$K_2(LA)_x$ ($x = 6, 8, 10, 12$)	Chain length dependence of secondary structure in monolayers and bulk phases, dependence of secondary structure on spreading conditions	78

Table 3. (*continued*)

Molecular class	Specific molecule(s)	Structural information	References
	Amphipathic synthetic peptides	Chain length dependence of secondary structure and orientation; comparison of conformation in bulk, transferred films, and monolayers	24, 25, 86, 87
Acylamino acids	*N*-octadecanoyltyrosine (and its methyl ester)	Effects of hydrogen-bonding and metal complexation	56
	Octadecanoylserine methyl ester	Protonation state of C=O, chirality	57
	N-hexadecanoylalanine	Effect of pH and temperature on conformational ordering, effects of metal ions and chirality on intermolecular interactions	58
Polymers	Alanine and 2-aminobutyric acid-containing polymers	Orientation of helices	64
	Dodecylcellulose	Film orientation, effects of spreading methods	65
	Poly(*p*-phenylenevinylenes)	Orientation of aromatic ring and ether groups	66
	Polyoxazoline lipopolymers	Systematic studies of conformational ordering	67, 68
Miscellaneous	Barbituric acid lipids and amino-containing molecules	Hydrogen bonding network	69, 70

DSPC, 1,2-distearoylphosphatidylcholine; DMPC, 1,2-dimyristoylphosphatidylcholine; POPC, 1-palmitoyl-2-oleoylphosphatidylcholine; OPPC, 1-oleoyl-2-palmitoylphosphatidylcholine; DPPC-d_{62}, perdeuterated DPPC; DPPS, 1,2-dipalmitoylphosphatidylserine; DMPA, dimyristoylphosphatidic acid.

Table 4. Summary of experimental approaches to IRRAS.

Experimental Approach	Advance	References
Interfacing IR spectrometer to Langmuir trough	$\pi-A$ isotherms and IRRAS	71
PM-IRRAS	Theory and experiment, optimal angle of incidence	9, 72–74
Sample shuttling	Compensates for water vapor allowing quantitative analysis in IR regions rich in structural information	7, 21
Insertion of optical filter	Minimization of local heating	6
Influence of spreading solvent and techniques	Comparison on long chain molecules	11, 12

of confidence in the result. For a 45° angle of incidence, the intensity of the p-polarized component reverses sign at a helix tilt angle of ~25°. Furthermore, the band exhibits a distorted shape (derivative-like feature) at tilt angles from ~20 to 40°. Thus the simple fact that the p-polarized component has a negative RA with little band distortion establishes immediately that the molecule is not perpendicular to the surface. The detailed analysis outlined above (equations 1–14) is utilized to determine the exact orientation.

Ulrich and Vogel[23] have used PM-IRRAS to examine gramicidin A/lipid monolayers at a single angle of incidence (75°) along with simulations of the band contour to conclude that at low surface pressures, the helix lies flat on the surface, whereas at high pressures the helix was almost parallel to the surface normal. It seems fair to reiterate that measurements at several incident angles would improve the accuracy available in the tilt angle determination by IRRAS, as noted above. These two studies represent the only attempts at quantitative determination of peptide orientation to date. Qualitative evaluations of helix orientation at the air–water interface have been conducted using PM-IRRAS at a single incident angle by comparing Amide I to Amide II band intensities.[24,25]

2.6 Applications of IRRAS

A fairly comprehensive summary of IRRAS applications is presented in Tables 3 and 4. Rather than offering a one sentence recapitulation of each work, we have chosen to refer the interested reader to the original citation for elaboration.

2.7 Future prospects

A variety of technical advances to be introduced in the next few years will enhance the quantitative aspects of IRRAS. As noted above, it is essential to make measurements at several angles of incidence for accurate tilt

angle determination. With current instrumentation, this is a time-consuming procedure, since the optical system and monolayer have to be dismantled and reassembled between measurements. To do this, the purge has to be broken. Thus it takes at best about a day to make measurements at a single angle of incidence. To acquire reproducible data (in triplicate) at four or five angles of incidence and two polarizations therefore requires at least a month.

To overcome the above technical difficulties, Bruker Instruments has recently marketed an IR reflectance accessory in which the angle of incidence may be adjusted under computer control from 30 to 70°, thereby removing the need to break down the experiment for different angles of incidence. In Figure 9 IRRAS intensity measurements (s- and p-polarization) at 20 angles of incidence between 30° and 70° are plotted for the symmetric stretching vibrations of acyl-chain perdeuterated DPPC (DPPC-d_{62}). These data were collected in less than one day and provide a large improvement in both the speed of data acquisition and the accuracy of the measured tilt angle. The best fit to the data in Figure 9 are shown by the solid line which represents a tilt angle of 26°. The general availability of this device will clearly enhance the ease of tilt angle determination.

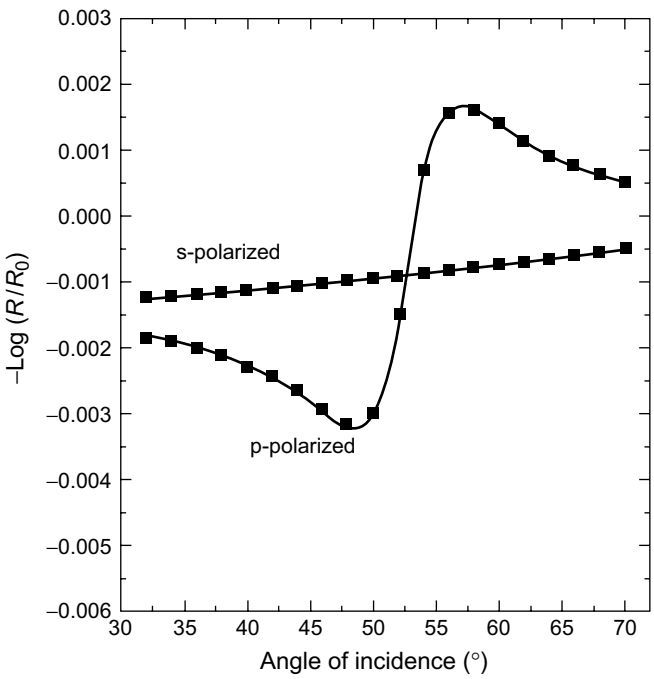

Figure 9. Measured (■) and calculated (—) reflectance–absorbance ($-\log(R/R_o)$) values versus angle of incidence for the ν_s CD_2 vibrational mode of a pure DPPC-d_{62} monolayer on an H_2O subphase at 21 °C and at a surface pressure of 28 mN m^{-1}. The best fit to the data was found using an acyl chain tilt angle of 26°. The calculated lines and experimental data sets for s- and p-polarized light are shown. (Figure courtesy of Professor Arne Gericke, Kent State University.)

General spectroscopic advances will also find their applicability in IRRAS. Detectors such as arsenic-doped silicon offer the potential for substantial gains in range and sensitivity compared to the mercury cadmium telluride devices used currently. A small drawback of these is the necessity to work at liquid helium temperatures. In addition, the development of tunable IR lasers ought to enhance the sensitivity of IRRAS by providing orders of magnitude more source intensity. The price one will have to pay (both in currency and in technical issues such as surface heating) remains to be evaluated. Finally, the coordination of IRRAS measurements of molecular conformation and orientation with other technologies which provide information at different distance scales (Brewster angle microscopy, fluorescence microscopy, X-ray) will provide a complete understanding of monolayer structure.

ACKNOWLEDGMENT

The work described from Rutgers University has been supported from the Public Health Service through grant GM 29864 to RM. Their generosity is much appreciated. We thank Professor Arne Gericke for demonstrating the IR reflectance accessory and allowing us to show his data for DPPC-d_{62}.

ABBREVIATIONS AND ACRONYMS

ATR	Attenuated Total Reflection
DMPA	Dimyristoylphosphatidic Acid
DMPC	1,2-Dimyristoylphosphatidylcholine
DPPC	1,2-Dipalmitoylphosphatidylcholine
DPPC-d_{62}	Perdeuterated 1,2-dipalmitoylphosphatidylcholine
DPPS	1,2-Dipalmitoylphosphatidylserine
DSPC	1,2-Distearoylphosphatidylcholine
IRRAS	Infrared Reflection–Absorption Spectroscopy
OPPC	1-Oleoyl-2-palmitoylphosphatidylcholine
PM-IRRAS	Polarization Modulation Infrared Reflection–Absorption Spectroscopy
POPC	1-Palmitoyl-2-oleoylphosphatidylcholine
RA	Reflectance–Absorbance
RDS	Respiratory Distress Syndrome

REFERENCES

1. R.A. Dluhy and D.G. Cornell, *J. Phys. Chem.*, **89**, 3195 (1985).
2. R.A. Dluhy, *J. Phys. Chem.*, **90**, 1373 (1986).

3. R. Mendelsohn, J.W. Brauner and A. Gericke, *Ann. Rev. Phys. Chem.*, 305 (1995).
4. R.A. Dluhy, S.M. Stephens, S. Widayati and A.D. Williams, *Spectrochim. Acta (A)*, **51**, 1413 (1995).
5. D. Blaudez, T. Buffeteau, B. Desbat and J.M. Turlet, *Curr. Opin. Colloid Interface Sci.*, **4**, 265 (1999).
6. H. Sakai and J. Umemura, *Langmuir*, **13**, 502 (1997).
7. C.R. Flach, J.W. Brauner, J.W. Taylor, R.C. Baldwin and R. Mendelsohn, *Biophys. J.*, **67**, 402 (1994).
8. D. Blaudez, T. Buffeteau, J.C. Cornut, B. Desbat, N. Escafre, M. Pezolet and J.M. Turlet, *Thin Solid Films*, **242**, 146 (1994).
9. T. Buffeteau, B. Desbat and J.M. Turlet, *Appl. Spectrosc.*, **45**, 380 (1991).
10. N.R. Pallas and B.A. Pethica, *Langmuir*, **1**, 509 (1985).
11. A. Gericke, J. Simon-Kutscher and H. Hühnerfuss, *Langmuir*, **9**, 2119 (1993).
12. A. Gericke, J. Simon-Kutscher and H. Hühnerfuss, *Langmuir*, **9**, 3115 (1993).
13. C.R. Flach, A. Gericke and R. Mendelsohn, *J. Phys. Chem.(B)*, **101**, 58 (1997).
14. V.L. Kuzmin and A.V. Michailov, *Opt. Spectrosc.*, **51**, 383 (1981).
15. V.L. Kuzmin, V.P. Romanov and A.V. Michailov, *Opt. Spectrosc.*, **73**, 3 (1992).
16. H. Schopper, *Z. Phys.*, **132**, 146 (1952).
17. K. Yamamoto and H. Ishida, *Appl. Spectrosc.*, **48**, 775 (1994).
18. K. Yamamoto and H. Ishida, *Vib. Spectrosc.*, **8**, 1 (1994).
19. J.E. Bertie, M.K. Ahmed and H.H. Eysel, *J. Phys. Chem.*, **93**, 2210 (1989).
20. R.D.B. Fraser and T.P. MacRae, 'Conformation in Fibrous Proteins and Related Synthetic Polypeptides', Academic Press, New York (1973).
21. A. Gericke, C.R. Flach and R. Mendelsohn, *Biophys. J.*, **73**, 492 (1997).
22. K.J. Rothschild and N.A. Clark, *Biophys. J.*, **25**, 473 (1979).
23. W.-P. Ulrich and H. Vogel, *Biophys. J.*, **76**, 1639 (1999).
24. I. Cornut, B. Desbat, J.-M. Turlet and J. Dufourcq, *Biophys. J.*, **70**, 305 (1996).
25. S. Castano, B. Desbat, M. Laguerre and J. Dufourcq, *Biochim. Biophys. Acta*, **1416**, 176 (1999).
26. Y. Ren, C.W. Meuse, S.L. Hsu and H.D. Stidham, *J. Phys. Chem.*, **98**, 8424 (1994).
27. Y. Ren, M.S. Shoichet, T.J. McCarthy, H.D. Stidham and S.L. Hsu, *Macromolecules*, **28**, 358 (1995).
28. C. Alonso, D. Blaudez, B. Desbat, F. Artzner, B. Birge and A. Renault, *Chem. Phys. Lett.*, **284**, 446 (1998).
29. J.T. Buontempo and S.A. Rice, *J. Chem. Phys.*, **98**, 5835 (1993).
30. J.T. Buontempo and S.A. Rice, *J. Chem. Phys.*, **99**, 7030 (1993).
31. H. Sakai and J. Umemura, *Chem. Lett.*, **12**, 2167 (1993).
32. H. Sakai and J. Umemura, *J. Bull. Chem. Soc. Japan*, **70**, 1027 (1997).
33. H. Sakai and J. Umemura, *Langmuir*, **14**, 6249 (1998).
34. B.F. Sinnamon, R.A. Dluhy and G.T. Barnes, *Colloids and Surf., A*, **146**, 49 (1999).
35. H. Sakai and J. Umemura, *Chem. Lett.*, **1996**, 465 (1996).
36. A. Gericke and H. Hühnerfuss, *J. Phys. Chem.*, **97**, 12899 (1994).
37. A. Gericke and H. Hühnerfuss, *Ber. Bunsen. Phys. Chem.*, **99**, 641 (1995).
38. A. Gericke and H. Hühnerfuss, *Langmuir*, **11**, 225 (1995).
39. J. Simon-Kutscher, A. Gericke and H. Hühnerfuss, *Langmuir*, **12**, 1027 (1996).
40. A. Gericke and H. Hühnerfuss, *Thin Solid Films*, **245**, 74 (1994).
41. D. Blaudez, T. Buffeteau, N. Castings, B. Desbat and J.-M. Turlet, *J. Chem. Phys.*, **104**, 9983 (1996).
42. A. Gericke and R. Mendelsohn, *Langmuir*, **12**, 758 (1996).
43. C. Ohe, H. Ando, N. Sato, Y. Urai, M. Yamammoto and K. Itoh, *J. Phys. Chem. (B)*, **103**, 435 (1999).
44. M.L. Mitchell and R.A. Dluhy, *J. Am. Chem. Soc.*, **110**, 712 (1988).
45. R.A. Dluhy, N.A. Wright and P.R. Griffiths, *Appl. Spectrosc.*, **42**, 138 (1988).
46. R.A. Hunt, M.L. Mitchell and R.A. Dluhy, *J. Mol. Struct.*, **214**, 93 (1989).
47. A. Gericke, D.J. Moore, R. Erukulla, R. Bittman and R. Mendelsohn, *J. Mol. Struct.*, **379**, 227 (1996).
48. B. Pastrana-Rios, C.R. Flach, J.W. Brauner and R. Mendelsohn, *Biochemistry*, **33**, 5121 (1994).
49. C.R. Flach, J.W. Brauner and R. Mendelsohn, *Biophys. J.*, **65**, 1994 (1993).
50. A. Dicko, H. Bourque and M. Pézolet, *Chem. Phys. Lipids*, **96**, 125 (1998).
51. C.R. Flach, R. Mendelsohn, M.E. Rerek and D.J. Moore, *J. Phys. Chem.*, **104**, 2159 (2000).
52. B. Pastrana-Rios, S. Taneva, K.M.W. Keough, A.J. Mautone and R. Mendelsohn, *Biophys. J.*, **69**, 2531 (1995).
53. A. Gericke and H. Hühnerfuss, *Chem. Phys. Lipids*, **74**, 205 (1994).
54. M. Grandbois, B. Desbat, D. Blaudez and C. Salesse, *Langmuir*, **15**, 6594 (1999).
55. R.A. Dluhy, Z. Ping, K. Fuacher and J.M. Brockman, *Thin Solid Films*, **329**, 308 (1998).
56. H. Hühnerfuss, V. Neumann and K.J. Stine, *Langmuir*, **12**, 2561 (1996).
57. A. Gericke and H. Hühnerfuss, *Langmuir*, **10**, 3782 (1994).
58. F. Hoffman, H. Hühnerfuss and K.J. Stine, *Langmuir*, **14**, 4525 (1998).
59. C.R. Flach, F.G. Prendergast and R. Mendelsohn, *Biophys. J.*, **70**, 539 (1996).
60. F. Wu, C.R. Flach, B.A. Seaton, T.R. Mealy and R. Mendelsohn, *Biochemistry*, **38**, 792 (1999).

61. F. Wu, A. Gericke, C.R. Flach, T.R. Mearly, B.A. Seaton and R. Mendelsohn, *Biophys. J.*, **74**, 3273 (1998).
62. J. Gallant, B. Desbat, D. Vaknin and C. Salesse, *Biophys. J.*, **75**, 2888 (1998).
63. C.R. Flach, A. Gericke, K.M.W. Keough and R. Mendelsohn, *Biochim. Biophys. Acta*, **1416**, 11 (1999).
64. K. Fujita, S. Kimura, Y. Imanishi, E. Okamura and J. Umemura, *Langmuir*, **11**, 1675 (1995).
65. L. Mao, A.-M. Ritcey and B. Desbat, *Langmuir*, **12**, 4754 (1996).
66. J.G. Hagting, R.E.T.P. de Vos, K. Sinkovics, E.J. Vorenkamp and A.J. Schouten, *Macromolecules*, **32**, 3930 (1999).
67. T.R. Baekmark, T. Wiesenthal, P. Kuhn, T.M. Bayerl, O. Nuyken and R. Merkel, *Langmuir*, **13**, 5521 (1997).
68. T.R. Baekmark, T. Wiesenthal, P. Kuhn, A. Albersdorfer, O. Nuyken and R. Merkel, *Langmuir*, **15**, 3616 (1999).
69. M. Weck, R. Fink and H. Ringsdorf, *Langmuir*, **13**, 3515 (1997) .
70. Q. Huo, L. Dziri, B. Desbat, K.C. Russell and R.M. Leblanc, *J. Phys. Chem. B.*, **103**, 2929 (1999).
71. R.A. Dluhy, M.L. Mitchell, T. Pettenski and J. Beers, *Appl. Spectrosc.*, **42**, 1289 (1988).
72. T. Buffeteau, D. Blaudez, E. Péré and B. Desbat, *J. Phys. Chem. B.*, **103**, 5020 (1999).
73. D. Blaudez, J.M. Turlet, J. Dufourcq, D. Bard, T. Buffeteau and B. Desbat, *J. Chem. Soc. Faraday Trans.*, **92**, 525 (1996).
74. D. Blaudez, T. Buffeteau, B. Desbat, P. Fournier, A.-M. Ritcey and M.J. Pézolet, *J. Phys. Chem. B.*, **102**, 99 (1998).
75. S.A. Riou, S.L. Hsu and H.D. Stidham, *Biophys. J.*, **75**, 2451 (1998).
76. S.A. Riou, S.L. Hsu and H.D. Stidham, *Langmuir*, **14**, 3062 (1998).
77. H.J. Chen, S.L. Hsu, D.A. Tirrell and H.D. Stidham, *Langmuir*, **13**, 4775 (1997).
78. D. Dieudonné, A. Gericke, C.R. Flach, X. Jiang, R.S. Farid and R. Mendelsohn, *J. Am. Chem. Soc.*, **120**, 792 (1998).
79. V. Neumann, A. Gericke and H. Hühnerfuss, *Langmuir*, **11**, 2206 (1995).
80. R.N.A.H. Lewis, E.J. Prenner, L.H. Kondejewski, C.R. Flach, R. Mendelsohn, R.S. Hodges and R.N. McElhaney, *Biochemistry*, **38**, 15 193 (1999).
81. A. Gericke, A.V. Michailov and H. Hühnerfuss, *Vib. Spectrosc.*, **4**, 335 (1993).
82. C. Schladitz, E.P. Vieira, H. Hermel and H. Möhwald, *Biophys. J.*, **77**, 3305 (1999).
83. M. Weygand, M. Schalke, P.B. Howes, K. Kjaer, J. Friedmann, B. Wetzer, D. Pum, U.B. Sleytr and M. Lösche, *J. Mater. Chem.*, **10**, 141 (2000).
84. D. Blaudez, F. Boucher, T. Buffeteau, B. Desbat, M. Grandbois and C. Salesse, *Appl. Spectrosc.*, **53**, 1299 (1999).
85. H. Lavoie, J. Gallant, M. Grandbois, D. Blaudez, B. Desbat, F. Boucher and C. Salesse, *Mater. Sci. Eng., C*, **10**, 147 (1999).
86. M. Boncheva and H. Vogel, *Biophys. J.*, **73**, 1056 (1997).
87. S. Castano, B. Desbat and J. Dufourcq, *Biochim. Biophys. Acta*, **1463**, 65 (2000).